ID-Pose: Sparse-view Camera Pose Estimation by Inverting Diffusion Models

Weihao Cheng Yan-Pei Cao Ying Shan ARC Lab

whcheng@tencent.com caoyanpei@gmail.com yingsshan@tencent.com

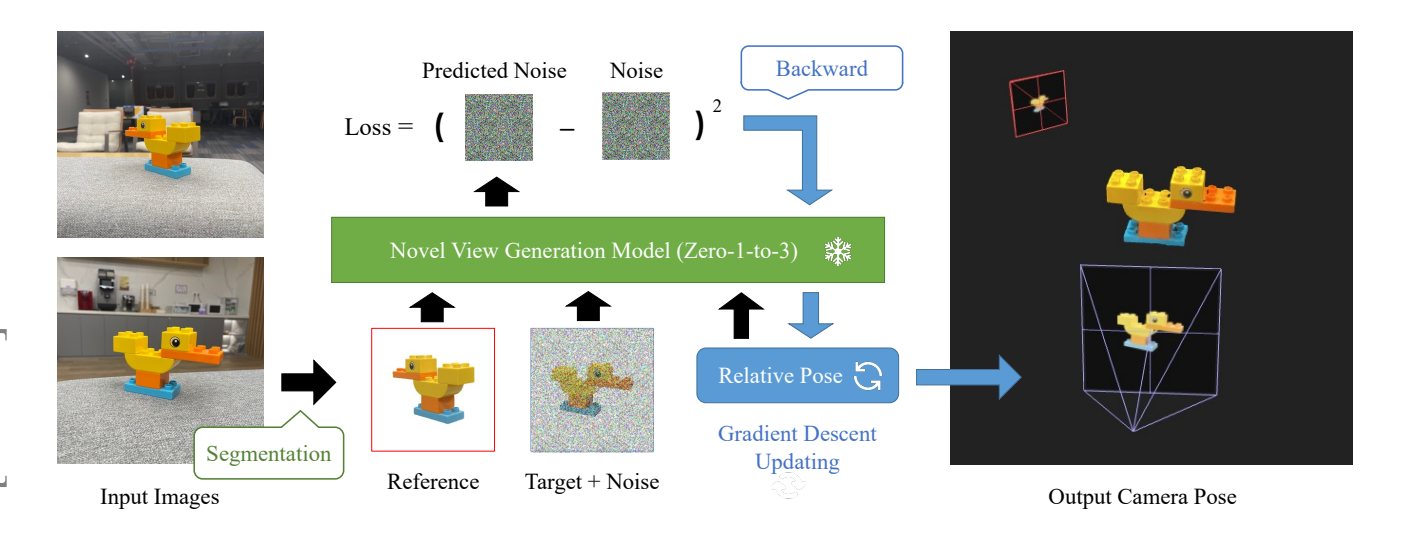


Figure 1. ID-Pose estimates the relative camera pose of two input images. It uses one image as a reference and the other image as the target, where the target image is added with Gaussian noise. Assume there is a relative transformation from the camera pose of the reference to the target. ID-Pose utilizes the noise predictor from Zero-1-to-3 [8] to compute the noise given the noisy target image, the reference image, and the relative pose. The prediction error is used as the objective of the relative pose in ID-Pose then applies the gradient descent method to find the optimal relative pose that connects the two views.

Abstract

Given sparse views of an object, estimating their camera poses is a long-standing and intractable problem. We harness the pre-trained diffusion model of novel views conditioned on viewpoints (Zero-1-to-3). We present ID-Pose which inverses the denoising diffusion process to estimate the relative pose given two input images. ID-Pose adds a noise on one image, and predicts the noise conditioned on the other image and a decision variable for the pose. The prediction error is used as the objective to find the optimal pose with the gradient descent method. ID-Pose can handle more than two images and estimate each of the poses with multiple image pairs from triangular relationships. ID-Pose requires no training and generalizes to real-world images. We conduct experiments using high-quality real-scanned

3D objects, where ID-Pose significantly outperforms state-of-the-art methods. https://xt4d.github.io/id-pose/.

1. Introduction

Estimating camera poses of images is an important task for 3D understanding, reconstruction [6,11,24], and generation [21]. Given sparse views of an object, it is often intractable to estimate their poses. Traditional methods such as Structural-from-Motion (SfM) [17] require dense local features [1,9,19] that are unavailable with sparsely sampled images. Recent methods train neural networks to directly predict poses given images [7,10,18,22]. However, the generalization ability of these methods is limited by the scale of training data, which requires expensive dense image collec-

tion [15] or exhaustive pose annotating [5].

We solve the camera pose estimation problem by harnessing the pre-trained diffusion model of novel views conditioned on viewpoints (Zero-1-to-3) [8]. We present ID-Pose which inverses the denoising diffusion process to estimate the relative pose of two input images. ID-Pose leverages the pre-trained diffusion model, and maintains the relative pose as the optimization variable. It is conditioned on one image and the pose to predict the noise added to the other image. The error of the prediction is used as the objective to update the pose with the gradient descent method. To prevent local minimum, we propose an initialization strategy that first samples a number of candidature poses with a few steps of optimization and then selects the one with the minimum prediction error of noise. We further extend ID-Pose to effectively find relative poses of more than two images. The idea is to estimate a pose with multiple image pairs. Within a group of three images, we can use the poses of two image pairs to present the pose of the third pair. Therefore, the prediction error of the third pair can be used to update the two poses alternately. ID-Pose is a zero-shot method that generalizes to open-world images by leveraging the diffusion model pre-trained on largescale data [8, 16]. We conduct experiments on high-quality real-scanned 3D objects, where ID-Pose significantly outperforms state-of-the-art methods.

2. Related Work

Camera Pose Estimation. Estimating camera poses of images is a long-standing problem. Traditional methods extract local features [1, 9, 19] of input images and find their matches to estimate poses. When images are sparsely captured, they often fail to estimate poses due to insufficient feature matches. Recent learning based methods [7, 10, 18, 22] use neural networks to predict the relative poses of image pairs. These methods require a large number of pose annotations, which are usually estimated with dense views of an object [15]. As training data is expensive to obtain, the neural networks are limited to benchmarks and hard to handle out-of-distribution images.

Image Diffusion Models. Diffusion models [4] have been widely used for image generation tasks. They learn a neural network to denoise an image, that takes a noisy image to predict the noise values mixed in the image. As the noise is random, the model essentially predicts the image and subtracts it from the noisy image to obtain the noise values. By progressive denoising from pure noise, a clear image can be generated. Latent diffusion models [16] denoise latent representations of images, which reduce the model complexity and improve the efficiency and stability. Recent models are able to condition on other inputs to control the generation, for example, natural language and sketches [12, 23]. Stable Diffusion [16] is a latent diffu-

sion model that generates high-quality images based on input texts by training on over a hundred million image-text pairs. A view-conditioned diffusion model, Zero-1-to-3 [8], uses one input image of an object and a relative pose to generate the novel view of the object under the new viewpoint. It is fine-tuned from Stable Diffusion with pose-annotated images rendered using Objaverse dataset [3]. It achieves prominent generation results with real-world images. We consider to inverse the denoising process of Zero-1-to-3, that uses two images of the same object to predict their relative camera pose. This enables zero-shot pose estimation given a sparse set of images.

3. Methodology

Our task is to estimate camera poses of images that are sparsely captured around an object. We present ID-Pose, a zero-shot method that takes two images as input and finds their relative camera pose. The idea is to invert the denoising process of the pre-trained novel view generation model, i.e., Zero-1-to-3 [8]. We extend ID-Pose to handle more than two images by inverting each of the poses with multiple image pairs. In this section, we first introduce the background knowledge of diffusion models, and then describe the details of the ID-Pose method.

3.1. Preliminary

Let x be an image, and z be the latent map of x. Given a Gaussian noise ϵ , one can add a small portion of ϵ to z stepby-step, and finally turn z into ϵ . At each step t, a noisy latent map $z(\epsilon,t)$ is obtained by mixing z and ϵ with proportion scales controlled by t. Latent diffusion models [16] learn a step-wise noise predictor $f(z(\epsilon,t),t)$ that predicts the noise added to $z(\epsilon,t)$. To generate an image, a latent diffusion model starts from a noise ϵ and assumes there is a z underlying the ϵ . It then predicts and removes the noise step-by-step. After a fixed number of steps, it recovers the latent map z, which is then input to an image decoder to obtain the resulting image.

Stable Diffusion [16] is a latent diffusion model that generates images conditioned on text. Its noise predictor is therefore written as $f(z(\epsilon,t),text,t)$. The condition text is mapped to CLIP [14] embedding tokens which are crossattended with the hidden states of the predictor network.

Zero-1-to-3 [8] is fine-tuned from Stable Diffusion that generates novel views of an object conditioned on a reference view x_c and a relative camera pose p. Its noise predictor is written as $f(z(\epsilon,t),x_c,p,t)$. The reference view x_c is mapped to image tokens with the CLIP image encoder. The camera pose p is expressed in a spherical coordinate system where the position of a point is specified by three numbers: polar angle, azimuth angle, and radius. The three values of the pose p are concatenated with the x_c tokens as conditions to the predictor f. Zero-1-to-3 is fine-tuned with

large-scale images rendered from 3D objects but generalizes to real-world images.

3.2. ID-Pose

Let $f(z(\epsilon), x, p)$ be the pre-trained noise predictor of Zero-1-to-3, where the diffusion step t is omitted for simple notations. Given two images x_0 and x_1 , we inverse the denoising process to estimate their relative pose, which is represented in spherical coordinates (polar, azimuth, radius). Let x_0 be the reference view and x_1 be the target view. We add a noise ϵ to x_1 and use f to predict the noise. Assume f is the pose transformation from f0 to f1, the predicted noise is defined as a function of f2:

$$\hat{\epsilon}(p; x_0, x_1) = f(z_1(\epsilon), x_0, p),$$
 (1)

where $z_1(\epsilon)$ is the noisy latent map of x_1 . We define the noise error of the prediction given p as:

$$l(p; x_0, x_1) = ||\hat{\epsilon}(p; x_0, x_1) - \epsilon||_2^2.$$
 (2)

We also consider that x_1 acts as the reference view and x_0 acts as the target view. Let p' be the reversed transformation of p (from x_1 to x_0). The predicted noise of p' is:

$$\hat{\epsilon}(p'; x_1, x_0) = f(z_0(\epsilon), x_1, p'), \tag{3}$$

where $z_0(\epsilon)$ is the noisy latent map of x_0 . The noise error of the prediction given p' is:

$$l(p'; x_1, x_0) = ||\hat{\epsilon}(p'; x_1, x_0) - \epsilon||_2^2.$$
 (4)

We randomly choose $l(p; x_0, x_1)$ or $l(p'; x_1, x_0)$ as the objective function g(p). The inversion process iteratively updates p by the gradient descent method:

$$p^{(k+1)} = p^{(k)} - \alpha \nabla g(p^{(k)}) \tag{5}$$

where α is the step factor, k represents the current updating step, and k+1 represents the next step. The iteration stops when p converges or k exceeds a maximum step count. The intuition is that, p reaches the optimum once the model can predict the noise with the minimum error.

The initialization of p is crucial as optimization can be often stuck into local minimums. For a near-symmetric object, the opposite view of one view can have the highest similarity among the other views. Under this situation, if p is initialized near the opposite view, it will be likely stuck into a local minimum. To alleviate this problem, we use a sampling approach to find reliable initialization. We uniformly sample a number of pose candidates on a sphere around the origin point. The relative radius of the candidature poses is set to zero. For each candidate, we update the pose for a few steps with Equation 5. We then evaluate those poses with the *pairwise error*:

$$l_{0,1}(p) = l(p; x_0, x_1) + l(p'; x_1, x_0),$$
(6)

which combines the two noise errors to measure the stability of p connecting x_0 and x_1 . From all the candidates, we pick the one with the minimum *pairwise error* as the initial pose and further update it until convergence.

3.3. ID-Pose with More Views

Given n (n>2) images, a naive strategy is breaking them into n-1 consecutive pairs, and inverting the pose for each of them independently. However, there are many unused image pairs that can help to find these poses. We consequently propose to estimate each of the relative poses with multiple image pairs from triangular relationships. Suppose the input images are $x_0, x_1, ..., x_{n-1}$, we maintain n-1 relative poses $p_1, p_2, ..., p_{n-1}$ as variables, where p_i represents the relative transformation from x_0 to x_i . Firstly, we describe the initialization process. For each p_i , we uniformly sample m candidates and update them with a few steps. Instead of picking the best one, we keep those candidates as a group $\{p_{i,u}|u\in[0,m)\}$. Given two poses p_i and p_j where $i\neq j$, we define their $triangular\ error$ as:

$$l_{i,0,j}(p_i, p_j) = l_{0,i}(p_i) + l_{0,j}(p_j) + l_{i,j}(p_i' + p_j), \quad (7)$$

where $p_i' + p_j$ is the relative transformation from x_i to x_j . The *triangular error* sums up three *pairwise errors*, which indicates the instability of poses p_i and p_j to connect views x_0, x_i, x_j . Then, given a candidate $p_{i,u}$ of p_i , we iterate the candidates $p_{j,v}$ of p_j and calculate *triangular errors* (m times). We define the minimum error of $p_{i,u}$ pairing with p_j as:

$$e_{i,u,j} = \min_{v \in [0,m)} l_{i,0,j}(p_{i,u}, p_{j,v}). \tag{8}$$

We obtain $e_{i,u} = \sum_{j \neq i} e_{i,u,j}$ as the instability of $p_{i,u}$. We select $p_{i,u}$ with lowest instability as the initialization of p_i .

Next, we describe the inversion process. Suppose all poses are initialized, we randomly pick two indices i and j where $0 \le i \ne j < n$. We consider three situations. If i = 0, we update p_j with the noise error $l(p_j; x_0, x_j)$. If j = 0, we update p_i with the noise error $l(p_i'; x_i, x_0)$. If both i > 0 and j > 0, we will have two poses p_i and p_j to update. We fix one and update the other with the noise error $l(p_i' + p_j; x_i, x_j)$.

4. Experiments

4.1. Experimental Settings

Data. We conduct experiments on two datasets: OmniObject3D [20] and Amazon Berkeley Objects (ABO) [2]. These datasets are only used for testing, and none of the experimental methods are trained on them. OmniObject3D is a dataset of high-quality real-scanned 3D objects. It includes 190 categories with 6,000 scanned objects. We select 12 categories "house", "chair", "table", "bed", "ornaments", "shoe", "scissor", "guitar", "laundry detergent",

	Initialization Stage	Optimization Stage
Noise ϵ	fixed	random (each iteration)
Noise level	0.8	0.8
Step factor α	10.0	1.0
Batch size	16	1
Iterations	10 (each pose)	$600 \times (n-1)$

Table 1. The hyper-paramters of ID-Pose.

"dumbbell", "dinosaur", and "glasses". We select the first 5 scanned objects for each category if available. The total number of objects is 54. For each object, we use all the Blender rendered images as a view pool, and change their background color to white. ABO is a dataset of 3D Amazon.com products. We select 10 representative objects: "bag", "bar stool chair", "ergonomic chair", "sofa", "couch", "desk", "shelf", "bed", "fan", and "lamp". For each object, we place its geometry center at the origin point. We then setup a camera with FOV=60° looking at the origin, and randomly place it on a sphere to render 30 images. The radius of the sphere is set to a value that the object can be fully captured with enough image margin. The background is set to white during rendering. The rendered images form a view pool of an object. The ground truth poses are known and associated with the images. Given a view pool, we randomly pick out n images as a testing sample. We experiment with n = 2, 4, 6, 8. For OmniObject3D, we repeat the picking 3 times. We make 648 testing samples in total containing 2,592 relative poses to estimate. For ABO, we repeat the picking 10 times. We make 400 testing samples in total containing 1,600 relative poses to estimate.

Baseline Settings. We use RelPose++ [7] as the baseline method, which is trained using Common Objects 3D (v2) dataset [15]. There are two released model checkpoints. One is trained using raw images, the other is trained using masked images with clean background. We evaluate both of them in the experiments.

ID-Pose Settings. We use the checkpoint of Zero-1-to-3 [8] trained with 105000 iterations. We preprocess input images to have white background and contain enough margin, which fit the input distribution of the noise predictor. Given an image, we use a segmentation mask to clear the background, and use a window to crop out the object at its center. The size of the window is initially set to the largest bounding box of segmentation masks of all input images. The size is then scaled 1.5x to ensure that there is enough margin in the cropped images. The hyper-parameters used in ID-Pose are shown in Table 1. We additionally test ID-Pose without using triangular relationships.

Metrics. Given n images and the camera pose of one image. We estimate relative poses and obtain the poses for the other n-1 images. The poses are transformed into world

coordinate system. Following RelPose++ [7], we obtain relative rotations of the estimated poses and compute the angular differences to the ground truth relative rotations. We report the rotation accuracy which is the proportion of the angular differences less than 15 or 30 degree. We also compute the l_2 distances from the estimated camera positions to the ground truth positions. The distances are normalized by dividing the corresponding ground truth radius. We report the camera position accuracy which is the proportion of distances less than 20%.

4.2. Evaluation Results

We report evaluation results aggregated by the number of input views. The results on OmniObject3D and ABO samples are shown in Table 2 and Table 3, respectively. ID-Pose methods significantly outperform RelPose++ for all different n, which demonstrate advanced generalization capability. RelPose++ methods report much lower metrics compared to the testing results on the CO3D dataset [7]. The reason might be that the models of RelPose++ overfit to CO3D data and fail to generalize to out-of-distribution images. With two input images (n=2), ID-Pose w/o Tri and ID-Pose report the same results as they behave identically. With more input images (n>2), ID-Pose outperforms ID-Pose w/o Tri as extra image pairs are used to estimate poses. By adding input images, the performance of ID-Pose increase as more image pairs are used.

We visualize examples of estimated camera poses in the world coordinate system. We compare ID-Pose and Relpose++ with ground truth. Assume that the true camera pose of the reference image is known. For RelPose++, we transform all predicted poses with a matrix that aligns the first prediction to the reference. In Figure 2, we input four views of the "house_001" from OmniObject3D, where the front view acts as the reference. Compared with the ground truth, ID-Pose finds all three relative poses with small errors. RelPose++ accurately predicts the relative poses of the two side views, but makes a large prediction error on the opposite view. In Figure 3, we input four views of the "ornaments_001" from OmniObject3D, where the "left-face" view acts as the reference. This is a hard case for both ID-Pose and RelPose++. ID-Pose finds the approximate poses but with large errors compared to the ground truth. Rel-Pose++ predicts poses with even larger errors. In Figure 4, we input four views of an ABO chair object. ID-Pose accurately finds the camera poses, while RelPose++ fails to distinguish the differences between these images. This failure happens to almost all the ABO testing samples. RelPose++ is probably hard to handle out-of-distribution images. This exposes the weakness of the fitting based methods, that the generalization capability is limited by the amount of annotated training data. ID-Pose leverages the model pre-trained on large-scale images, which demonstrates better general-

		n = 2			n = 4			n = 6			n = 8	
Method	15°	30°	PA									
RelPose++ w/o Mask	5.56	14.20	8.64	4.12	12.35	7.20	3.70	12.72	8.27	4.41	12.61	9.08
RelPose++	6.17	11.11	12.96	4.32	11.73	12.76	3.70	11.85	11.60	4.50	11.90	11.46
ID-Pose w/o Tri	48.77	56.79	45.06	48.77	59.88	44.65	48.77	60.25	44.57	49.65	61.38	45.06
ID-Pose	48.77	56.79	45.06	49.79	61.11	46.50	50.12	63.33	46.42	52.38	65.26	48.06

Table 2. Results on the OmniObject3D testing samples. " 15° ": rotation accuracy by 15° . " 30° ": rotation accuracy by 30° . "PA": camera position accuracy. The numbers are shown in 100%.

		n = 2			n=4			n = 6			n = 8	
Method	15°	30°	PA	15°	30°	PA	15°	30°	PA	15°	30°	PA
RelPose++ w/o Mask	2.00	6.00	2.00	2.00	7.33	1.67	3.00	7.40	3.20	2.86	7.86	3.43
RelPose++	2.00	6.00	1.00	2.00	7.00	1.67	4.00	7.60	4.00	3.43	7.29	3.86
ID-Pose w/o Tri	76.00	80.00	73.00	75.00	78.33	74.00	77.60	80.00	75.60	77.71	80.57	75.86
ID-Pose	76.00	80.00	73.00	77.00	79.33	74.00	78.00	81.40	75.60	78.71	82.14	77.14

Table 3. Results on the ABO testing samples.

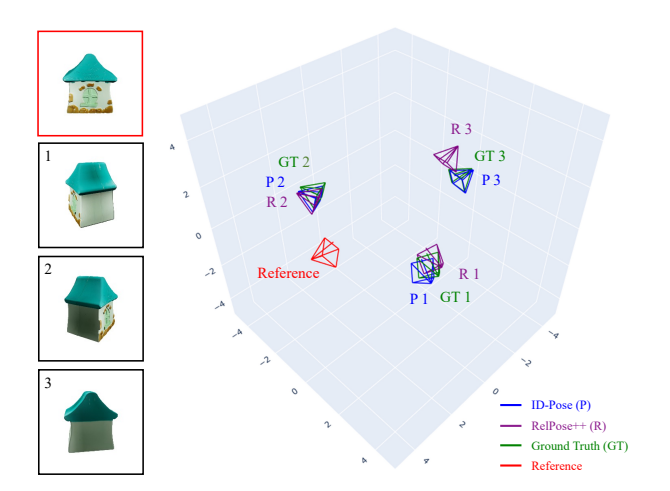
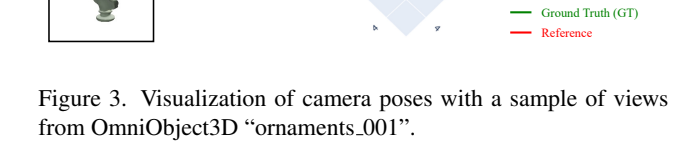


Figure 2. Visualization of camera poses with a sample of views from OmniObject3D "house_001".



RelPose++ (R)

ization ability.

4.3. Qualitative Results on In-the-wild Images

We qualitatively show the results of ID-Pose on in-the-wild images. We find three objects in our daily workplace: a toy duck, a chair, and a foosball table. We use a smartphone to capture 4-6 images for each of them. We use the DIS method [13] to segment out the objects and clean the background of the images to white. We select $n \ (n = 2, 3, 4)$ images as input views to estimate the relative poses. To visualize the results, we use the LumaAI APP¹ to reconstruct

3D meshes of the objects. We then choose one image as the reference and manually find its camera pose using the 3D mesh. With the ground truth camera pose of the reference image, we transform the estimated poses of the target views into the world coordinate system. We show an example of the results of the chair in Figure 5. More results can be interactively visualized on the project website². The estimated poses cannot align the views to the 3D object perfectly. One reason is that the true cameras may not look at the same point in the world, and their "up" vectors can be varied. For in-the-wild images, pose estimation with the as-

¹https://lumalabs.ai/

²https://xt4d.github.io/id-pose/

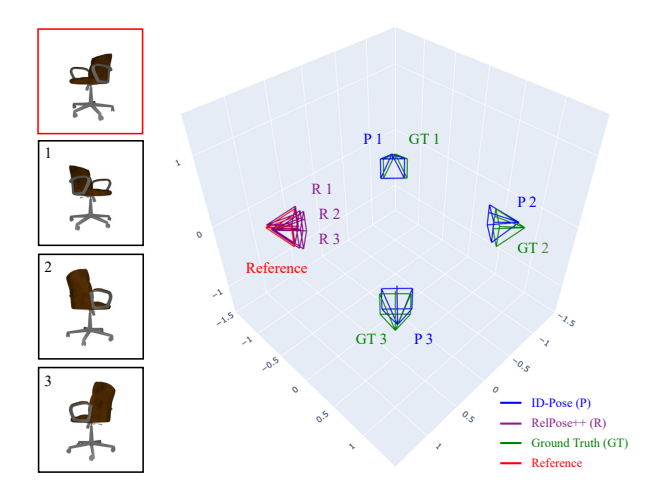


Figure 4. Visualization of camera poses with a sample of views from an ABO chair.



Figure 5. Visualization of estimated camera poses of sparsely captured views around a chair. The mesh is reconstructed using LumaAI APP. The view in red acts as the reference view, where the camera pose is manually found using the mesh.

sumption of spherical coordinates will introduce additional errors. This is a weakness of ID-Pose.

5. Conculsion & Limitations

In this paper, we propose ID-Pose which inverses the denoising diffusion process to estimate camera poses of sparse input views. ID-Pose only utilizes the pre-trained Zero-1-to-3 model [8] without additional training. Given two images, ID-Pose adds a noise on one image, and predicts the noise conditioned on the other image and a decision variable for the relative pose. The prediction error is used as the objective to find the optimal pose with the gradient descent method. ID-Pose can handle more than two images. It estimates each of the poses with additional pairs of images from triangular relationships. We conduct experiments using high-quality real-scanned 3D objects, where ID-Pose significantly outperforms state-of-the-art methods.

Limitations. The running time of ID-Pose is signifi-

cantly higher than neural fitting based methods. It requires multiple steps of pose updating by inference through large diffusion networks. The average time for running 100 steps is about 30 seconds on an NVIDIA V100 GPU. This is time-consuming and the method needs efficiency improvement. Due to the limitation of Zero-1-to-3, ID-Pose assumes that all cameras look at the same point and have no rotation around optical direction. This will introduce estimation errors for in-the-wild images. To extend the capability, one possible solution is to fine-tune the novel view diffusion model with the input of 6DOF poses rather than spherical coordinates.

References

- [1] Herbert Bay, Tinne Tuytelaars, and Luc Van Gool. Surf: Speeded up robust features. In *ECCV*, page 404–417, 2006.
- [2] Jasmine Collins, Shubham Goel, Kenan Deng, Achleshwar Luthra, Leon Xu, Erhan Gundogdu, Xi Zhang, Tomas F Yago Vicente, Thomas Dideriksen, Himanshu Arora, Matthieu Guillaumin, and Jitendra Malik. Abo: Dataset and benchmarks for real-world 3d object understanding. CVPR, 2022. 3
- [3] Matt Deitke, Dustin Schwenk, Jordi Salvador, Luca Weihs, Oscar Michel, Eli VanderBilt, Ludwig Schmidt, Kiana Ehsani, Aniruddha Kembhavi, and Ali Farhadi. Objaverse: A universe of annotated 3d objects. In CVPR, pages 13142– 13153, 2023. 2
- [4] Jonathan Ho, Ajay Jain, and Pieter Abbeel. Denoising diffusion probabilistic models. *NeurIPS*, 33:6840–6851, 2020.
- [5] Varun Jampani, Kevis-Kokitsi Maninis, Andreas Engelhardt, Arjun Karpur, Karen Truong, Kyle Sargent, Stefan Popov, Andre Araujo, Ricardo Martin-Brualla, Kaushal Patel, Daniel Vlasic, Vittorio Ferrari, Ameesh Makadia, Ce Liu, Yuanzhen Li, and Howard Zhou. Navi: Categoryagnostic image collections with high-quality 3d shape and pose annotations. 2023. 2
- [6] Hanwen Jiang, Zhenyu Jiang, Kristen Grauman, and Yuke Zhu. Few-view object reconstruction with unknown categories and camera poses. ArXiv, 2212.04492, 2022. 1
- [7] Amy Lin, Jason Y Zhang, Deva Ramanan, and Shubham Tulsiani. Relpose++: Recovering 6d poses from sparse-view observations. arXiv preprint arXiv:2305.04926, 2023. 1, 2, 4
- [8] Ruoshi Liu, Rundi Wu, Basile Van Hoorick, Pavel Tok-makov, Sergey Zakharov, and Carl Vondrick. Zero-1-to-3: Zero-shot one image to 3d object. arXiv preprint arXiv:2303.11328, 2023. 1, 2, 4, 6
- [9] David G. Lowe. Distinctive image features from scale-invariant keypoints. *IJCV*, page 91–110, 2004. 1, 2
- [10] Iaroslav Melekhov, Juha Ylioinas, Juho Kannala, and Esa Rahtu. Relative camera pose estimation using convolutional neural networks. In *ACIVS*, pages 675–687. Springer, 2017. 1, 2

- [11] Ben Mildenhall, Pratul P. Srinivasan, Matthew Tancik, Jonathan T. Barron, Ravi Ramamoorthi, and Ren Ng. Nerf: Representing scenes as neural radiance fields for view synthesis. In ECCV, page 405–421, 2020. 1
- [12] Chong Mou, Xintao Wang, Liangbin Xie, Jian Zhang, Zhongang Qi, Ying Shan, and Xiaohu Qie. T2i-adapter: Learning adapters to dig out more controllable ability for text-to-image diffusion models. arXiv preprint arXiv:2302.08453, 2023. 2
- [13] Xuebin Qin, Hang Dai, Xiaobin Hu, Deng-Ping Fan, Ling Shao, and Luc Van Gool. Highly accurate dichotomous image segmentation. In ECCV, 2022. 5
- [14] Alec Radford, Jong Wook Kim, Chris Hallacy, Aditya Ramesh, Gabriel Goh, Sandhini Agarwal, Girish Sastry, Amanda Askell, Pamela Mishkin, Jack Clark, et al. Learning transferable visual models from natural language supervision. In *ICML*, pages 8748–8763. PMLR, 2021. 2
- [15] Jeremy Reizenstein, Roman Shapovalov, Philipp Henzler, Luca Sbordone, Patrick Labatut, and David Novotny. Common objects in 3d: Large-scale learning and evaluation of real-life 3d category reconstruction. In CVPR, pages 10901– 10911, 2021. 2, 4
- [16] Robin Rombach, Andreas Blattmann, Dominik Lorenz, Patrick Esser, and Björn Ommer. High-resolution image synthesis with latent diffusion models. In CVPR, pages 10684– 10695, 2022. 2
- [17] Johannes L. Schonberger and Jan-Michael Frahm. Structurefrom-motion revisited. In CVPR, 2016. 1
- [18] Samarth Sinha, Jason Y Zhang, Andrea Tagliasacchi, Igor Gilitschenski, and David B Lindell. Sparsepose: Sparseview camera pose regression and refinement. In *CVPR*, pages 21349–21359, 2023. 1, 2
- [19] E. Tola, V. Lepetit, and P. Fua. Daisy: An efficient dense descriptor applied to wide-baseline stereo. *TPAMI*, 32(5):815–830, 2010. 1, 2
- [20] Tong Wu, Jiarui Zhang, Xiao Fu, Yuxin Wang, Jiawei Ren, Liang Pan, Wayne Wu, Lei Yang, Jiaqi Wang, Chen Qian, et al. Omniobject3d: Large-vocabulary 3d object dataset for realistic perception, reconstruction and generation. arXiv preprint arXiv:2301.07525, 2023. 3
- [21] Alex Yu, Vickie Ye, Matthew Tancik, and Angjoo Kanazawa. pixelnerf: Neural radiance fields from one or few images. In CVPR, 2021. 1
- [22] Jason Y Zhang, Deva Ramanan, and Shubham Tulsiani. Rel-pose: Predicting probabilistic relative rotation for single objects in the wild. In *ECCV*, pages 592–611. Springer, 2022.

 1, 2
- [23] Lvmin Zhang and Maneesh Agrawala. Adding conditional control to text-to-image diffusion models, 2023. 2
- [24] Zhizhuo Zhou and Shubham Tulsiani. Sparsefusion: Distilling view-conditioned diffusion for 3d reconstruction. In CVPR, pages 12588–12597, 2023. 1